3D optical nanoscopy with excited state saturation at liquid helium temperatures

J.-B Trebbia, R Baby, P. Tamarat, B. Lounis

▶ **To cite this version:**

J.-B Trebbia, R Baby, P. Tamarat, B. Lounis. 3D optical nanoscopy with excited state saturation at liquid helium temperatures. Optics Express, In press. hal-02186046

HAL Id: hal-02186046
https://hal.science/hal-02186046

Submitted on 17 Jul 2019

HAL is a multi-disciplinary open access archive for the deposit and dissemination of scientific research documents, whether they are published or not. The documents may come from teaching and research institutions in France or abroad, or from public or private research centers.

L'archive ouverte pluridisciplinaire **HAL**, est destinée au dépôt et à la diffusion de documents scientifiques de niveau recherche, publiés ou non, émanant des établissements d'enseignement et de recherche français ou étrangers, des laboratoires publics ou privés.

HAL
archives-ouvertes.fr

3D optical nanoscopy with excited state saturation at liquid helium temperatures

J.-B Trebbia, R Baby, P. Tamarat, B. Lounis

▶ **To cite this version:**

J.-B Trebbia, R Baby, P. Tamarat, B. Lounis. 3D optical nanoscopy with excited state saturation at liquid helium temperatures. Optics Express, Optical Society of America, In press. hal-02186046

HAL Id: hal-02186046
https://hal.archives-ouvertes.fr/hal-02186046

Submitted on 17 Jul 2019

HAL is a multi-disciplinary open access archive for the deposit and dissemination of scientific research documents, whether they are published or not. The documents may come from teaching and research institutions in France or abroad, or from public or private research centers.

L'archive ouverte pluridisciplinaire **HAL**, est destinée au dépôt et à la diffusion de documents scientifiques de niveau recherche, publiés ou non, émanant des établissements d'enseignement et de recherche français ou étrangers, des laboratoires publics ou privés.

3D optical nanoscopy with excited state saturation at liquid helium temperatures

J.-B. TREBBIA[1,2], R. BABY[1,2], P. TAMARAT[1,2], B. LOUNIS[1,2]*

1- Univ Bordeaux, LP2N, F- 33405 Talence, France
2- Institut d'Optique & CNRS, LP2N, F-33405 Talence, France
**blounis@u-bordeaux.fr*

Abstract: We present a 3D fluorescence nanoscopy method operating at cryogenic temperatures, based on optical saturation of the excited state of individual molecules. Using a focused laser beam structured with a zero-intensity central region surrounded by intensity gradients in the three space directions, we achieve a sub-30 nm 3D optical resolution. Moreover, the analysis of the fluorescence scanning images of single molecules reveals the 3D orientation of their transition dipole with an accuracy of a few degrees. This method provides a valuable tool for locating neighboring molecules with overlapping optical transitions in order to study their interactions.

1. Introduction

Hybrid systems formed by quantum emitters strongly coupled to photonic or plasmonic nanostructures are promising elementary building blocks for the realization of integrated solid-state quantum photonics devices[1,2]. In order to characterize and optimize the interactions between the emitters and the electromagnetic modes strongly confined within these nanostructures, it is crucial to develop simple optical techniques for nanometric localization of single emitters in the vicinity of these structures[3-5]. Such techniques could also be used to study arrays of interacting quantum emitters and control their mutual coupling that occur at the nanometer scale. They are thus of prime importance for the development of quantum information protocols based on networks of strongly interacting qubits[6].

Solid-state quantum emitters such as single molecules[7], quantum dots[8,9] and defect centers in diamond[10] are appealing candidates for the realization of such quantum networks. Among them, polycyclic aromatic hydrocarbon molecules embedded in well-chosen solid matrices at liquid helium temperatures behave as simple two-level systems, with a fluorescence quantum yield close to unity. Vanishing dephasing of their transition dipole by phonon-assisted processes leads to a large absorption cross-section at their zero-phonon line (ZPL), whose linewidth reaches its fundamental lower bound determined by the inverse lifetime of the emitting state[11]. It is also manifested in the indistinguishability of the single photons emitted on the ZPL[12]. Over the past years, single molecules have proven to be test-bench systems for quantum optics[12-17] and for the study of coherent optical dipole–dipole interactions[18]. Moreover, their photostability is excellent, with no blinking and no spectral diffusion even at high illumination intensities and over days[19].

Super-resolution[20,21] of single polycyclic-aromatic hydrocarbon molecules at cryogenic temperatures has been demonstrated with far-field optics, using two approaches based on the spectral selection of single molecules resonantly excited at their sharp ZPL. The simplest approach is based on successive localizations of single molecule fluorescence spot centers on a camera, while tuning the excitation laser frequency[22]. This method can hardly be employed to super-resolve molecules with overlapping resonances, i.e. molecules that can efficiently couple. The second is a very sophisticated method, which combines scanning of a

micro-electrode probe that creates a local inhomogeneous electric field and Stark-shift mapping of the single molecule ZPLs[18]. Recently, a simple 2D optical nanoscopy technique has been developed to super-resolve single molecules with a sub-10 nm resolution[23]. It is based on excited state saturation (ESSat) of the molecules with a doughnut-shaped laser beam (i.e. in the first-order Laguerre-Gaussian). Yet, due to the vanishing intensity of the doughnut mode all along the optical axis, the longitudinal resolution remains similar to that of standard confocal microscopy. Taking this concept further, we use here a light structuration technique to produce a local zero-intensity focal spot with steep longitudinal and transverse intensity gradients. We demonstrate 3D-ESSat nanoscopy of single molecules with a longitudinal resolution of 30 nm. Additionally, we show that this method provides an accurate determination of the 3D orientation of the molecular transition dipoles. Altogether, it paves the way to the study and control of coherent interactions between single quantum emitters.

2. Experimental setup

The fluorescent molecules chosen in the experiment are dibenzanthanthrene (DBATT) molecules embedded in a thin film (thickness of few microns) made of either an octadecane Shpolskii matrix (ZPL at ~ 589 nm) or a naphthalene molecular crystal (ZPL at ~ 618 nm). We select the molecules for which the effects of spherical aberrations on the recorded excitation point spread function (PSF) are negligible, i.e. those located at a depth less than ~ 0.5 µm from the surface. They exhibit ZPLs with a FWHM linewidth of ~ 20 MHz at 2 K and weak saturation intensities I_s of a few W/cm^2. The experiment is based on a modified scanning confocal microscopy setup sketched in Fig. 1(a). To realize a local 3D zero-intensity at the focus of the objective, the phase of the excitation field is patterned with a 0-π circular phase mask[24]. Using a spatial light modulator (SLM), we generate a π-phase retardation in the central region of the parallel incident beam (see Fig. 1b). The phase distribution of the laser beam is set to $p/2\mathrm{sgn}[\sin(z_0 2p\cos y)], y$ where is the incidence angle and z_0 a key parameter that fixes the relative size of the phase-retarded area. z_0 is chosen so that destructive interferences occurring between phase retarded and non-retarded areas of the 0-π incident beam produce a 3D zero-intensity at the focus of the objective. This hollow focal spot is surrounded by comparable intensity gradients in the three space directions.

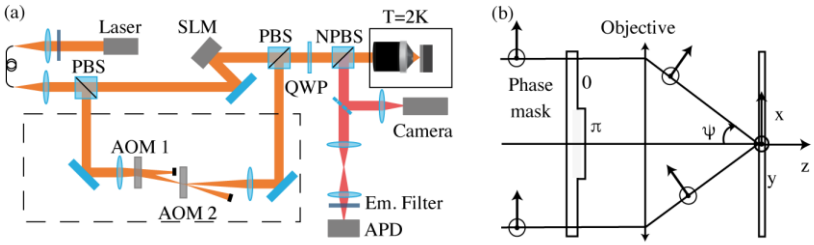

Fig. 1. (a) Schematic of the experimental setup. The beam of a single mode tuneable dye laser is sent to a SLM where the 0-π phase mask is imprinted. This beam is then passed through a quarter wave plate (QWP), which makes its polarization circular, and focused with a high numerical aperture objective (NA = 0.95) to excite the DBATT molecules on their ZPL. A piezoelectric stage scans the sample through the excitation PSF, while fluorescence emitted by the molecules is recorded with a single-photon-counting avalanche photodiode (APD). A CCD camera is used to characterize the beam spatial profile. The modulated-ESSat microscopy module is depicted in the dashed line box. The reflected beam from the first polarization beam splitter (PBS) is temporally modulated in intensity by two acoustic-optic modulators (AOM1 and 2), then recombined with the 0-π beam with the second PBS. (b) Schematic of the phase mask and the beam focusing, with the electric field orientations.

3. Simulation of fluorescence images

In order to illustrate the principle of 3D-ESSat nanoscopy, simulations of fluorescence images of a single molecule are presented in Fig. 2, assuming an isotropic molecular dipole orientation. We compute the three electric field components of the tightly focused laser beam near the focal point using the generalized vectorial Debye integral[25,26], which takes into account the phase distribution induced by the SLM and a factor of apodization $\sqrt{\cos(\gamma)}$ for energy conservation through the objective. The fluorescence image is calculated for a single emitter scanned through the focal region and excited at resonance. For laser intensities smaller than I_s, the fluorescence signal is proportional to the laser intensity and the images of the molecule reproduce the 3D local intensity distribution. When the intensity is increased, the saturation of the molecular transition leads to a broadening of the fluorescence (xy) and (xz) images and a sharpening of the central dark spots, therefore to a resolution enhancement in the focal (transverse) plane as well as along the optical (longitudinal) axis. We define the optical resolutions as the widths (FWHM) of the central dips in the cross sectional profiles of the scanned images (see Fig. 2b,c).

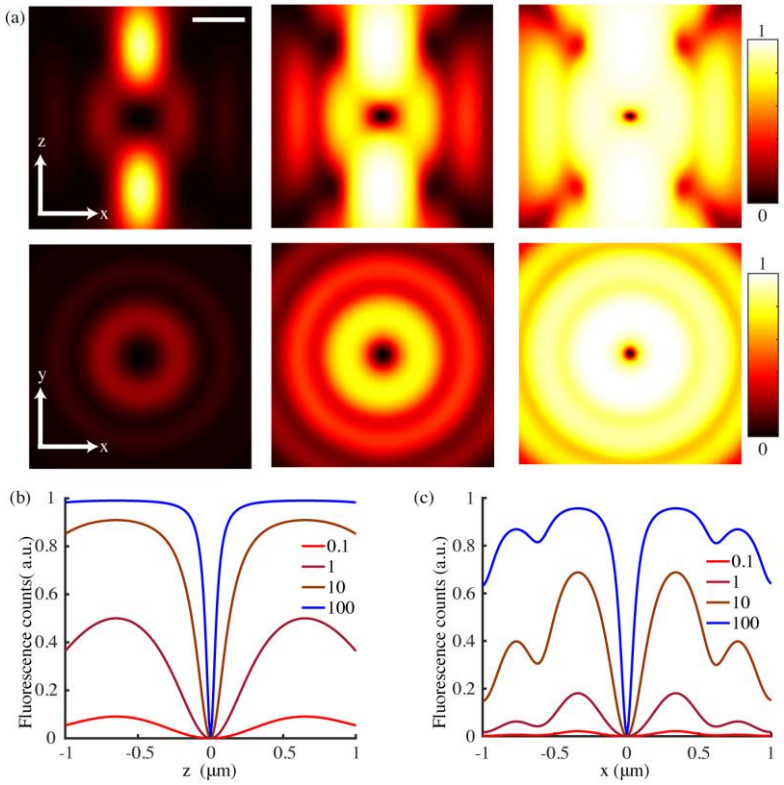

Fig. 2. (a) Simulated fluorescence images of a molecule excited with a circularly polarized 0-π beam (λ = 589 nm, z_0 = 0.68) and scanned through the PSF in the (xy) plane and in the (xz) plane for different saturation parameters I_{max}/I_S (0.1, 10, 100), where I_{max} is the maximum excitation intensity along z. The colorbar is normalized to the maximum fluorescence counts along the axis when I_{max}/I_S = 100. (b), (c) Cross-sectional profiles of the fluorescence signal along z (b), along x (c), for four values of I_{max}/I_s. In these simulations, the molecular dipole orientation is considered as isotropic. The computation of the three electric field components near the focal point is performed using the generalized vectorial Debye integral[25,26],

assuming that the molecules are close enough to the surface so that we can neglect the effects of beam propagation in the crystal and of Fresnel coefficients at the matrix surface.

In the linear regime, the large distances between the two longitudinal bright spots produce a poor resolution close to 610 nm at a laser wavelength λ = 589 nm, while the transverse resolution is close to 370 nm. Since the longitudinal intensity gradient is stronger than the transverse one, the longitudinal resolution becomes better than the transverse one at high excitation intensities, as shown in Fig. 3a. This results in a slightly anisotropic 3D PSF, with an aspect ratio of ~ 1.4 in the fully saturated regime.

4. Optical super-resolution

The laser intensity distribution along the optical axis in the central region of the PSF can be approximated as $I(z) = (I_{max} - I_{res})\sin^2(\pi z/d_z) + I_{res}$, where I_{res} is the residual intensity at the focus, I_{max} is the maximal intensity and d_z the separation between both intensity maxima along the axis. One can show that the longitudinal resolution improves as $1/\sqrt{I_{max}/I_S}$ at high saturation, and that the residual intensity inherent to real experiments sets the resolution limit:

$$\Delta z \approx \frac{2d_z}{\pi}\sqrt{\frac{1+I_{res}/I_S}{I_{max}/I_S}} \text{ for } I_{max} >> I_S \text{ and } I_{max} >> I_{res}.$$

Figure 3(b) presents the longitudinal resolution, computed for $I_{max} = 10^5 I_S$, as a function of I_{res} for d_z = 1300 nm (obtained at λ = 589 nm). It degrades as the residual intensity increases, so that a nanometric resolution requires extremely small values of I_{res}/I_{max}, below 10^{-4}. Achieving the best local zero-intensity by fine-tuning of the phase-mask parameter ζ_0 is therefore essential, as shown in Fig. 3(c).

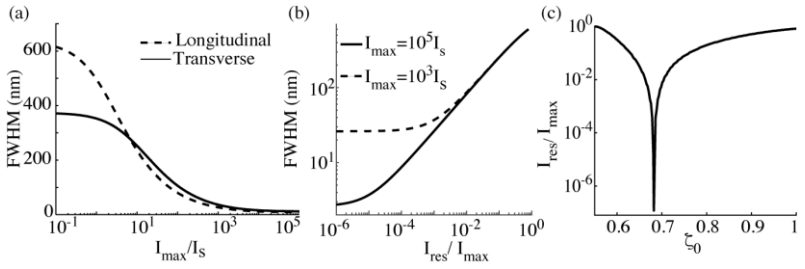

Fig. 3. (a) Computed longitudinal and transverse resolutions of 3D-ESSat microscopy as a function of the excitation intensity. These resolutions are derived from the simulated fluorescence intensity profiles. (b) Evolution of the longitudinal resolution as a function of the residual intensity at the center of the PSF for $I_{max}/I_S = 10^5$ (solid curve) and $I_{max}/I_S = 10^3$ (dashed curve). (c) Dependence of the residual intensity on the phase-mask parameter ζ_0. The minimum of I_{res} is obtained for $\zeta_0 = 0.68$. Its value of $10^{-7} I_{max}$ is here limited by finite discretization in the evaluation of the Debye integral. All simulations are performed with a laser wavelength λ = 589 nm.

In the experiment, the objective is inserted in the cryostat and undergoes mechanical strain at low temperature, which induces optical aberrations, mainly astigmatism. They are corrected by applying a set of well-chosen Zernike polynomials on the SLM[23,27]. After corrections,

I_{res} is reduced to $\sim 5 \times 10^{-3} I_{max}$. Fig. 4 (a)-(c) display 3D-ESSat images of a single DBATT molecule recorded in these conditions by scanning the sample in the planes (xy) and (xz) with three different laser intensities. For an excitation intensity of $I_{max} = 82$ W/cm^2 (see Fig. 4c), the longitudinal and transverse resolutions are 260 nm and 200 nm, respectively. For another molecule excited at higher intensity $I_{max} = 1.6$ kW/cm^2, the cross-sectional profiles displayed in Fig. 4 d,e demonstrate the achievement of transverse and longitudinal super-resolutions of 79 nm and 38 nm, respectively.

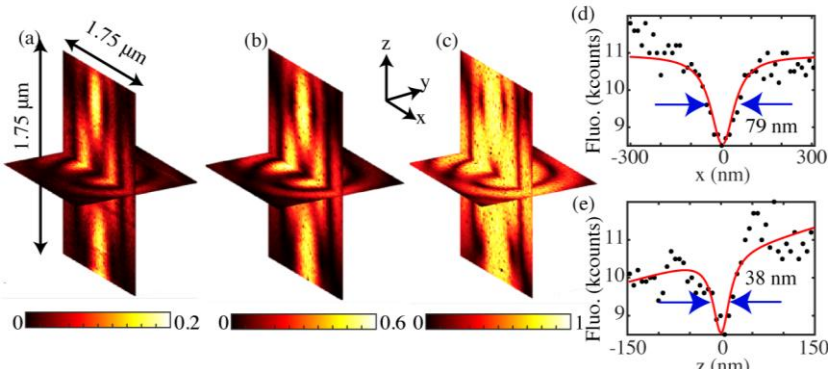

Fig. 4. 3D-ESSat fluorescence images of a single DBATT molecule embedded in octadecane at 2K, recorded in the (xy) and (xz) planes for three different excitation intensities: (a) I_{max} = 0.4 W/cm^2, (b) 16 W/cm^2 and (c) 82 W/cm^2. The pixel dwell time is 5 ms and the colorbar is normalized to the maximum fluorescence counts of (c). (d), (e) Cross sectional profiles along x and z for another molecule excited at I_{max} = 1.6 kW/cm^2. Their FWHM derived from Lorentzian fits (red curves) demonstrate 3D super-resolution. A slanted fluorescence background profile has been added to the fit to take into account the fluorescence signal from out-of-focus molecules.

5. 3D dipole orientation

Most of the applications introduced above will require the characterization of the exact 3D orientation of the molecular transition dipole. Various techniques have been developed to measure fixed or time-dependent single molecule dipole orientations[28]. They are based on selective polarization excitation schemes[29,30], dipole emission patterns[31] or scanning fluorescence images recorded under annular illumination and with different excitation polarizations[32]. Here, we combine the latter approach with ESSat nanoscopy. In the focal region, the high NA objective introduces a significant amount of polarization mixing such that the local electric field contains components of all directions, each of them having a specific spatial distribution[25]. A fluorescence scanning image of a molecule will consist in a characteristic combination of three intensity patterns corresponding to the three dipole projections. Comparing measured to simulated image patterns will therefore provide the 3D dipole orientation of a molecule.

Figure 5 shows a selection of simulated ESSat images built in the planes (xy), (xz) and (yz), for various polar angles θ of the molecular dipole placed in the (xz) plane. These images calculated at weak saturation $(I_{max} - I_s)$ reflect the squared projection of the laser field along the dipole. For instance, the three left (resp. right) images ($\theta = 90°$) gives the squared x-(resp. z) component of the field distribution. The (xy) images present a symmetry axis which is orthogonal to the in-plane dipole projection, except when the dipole is aligned along the z optical axis ($\theta = 0°$), in which case the revolution symmetry shows up. This axial symmetry can readily be used to determine the orientation of the in-plane dipole projection. Moreover,

variations in q lead to significant differences in the (xz) and (yz) images (see Fig. 5b,c), which can be exploited to retrieve the polar angle of the molecular dipole from the experimental images. In particular, we find that in the imaging plane (xz), the iso-intensity contour around the PSF center has an elongation axis that strikingly coincides with the dipole axis.

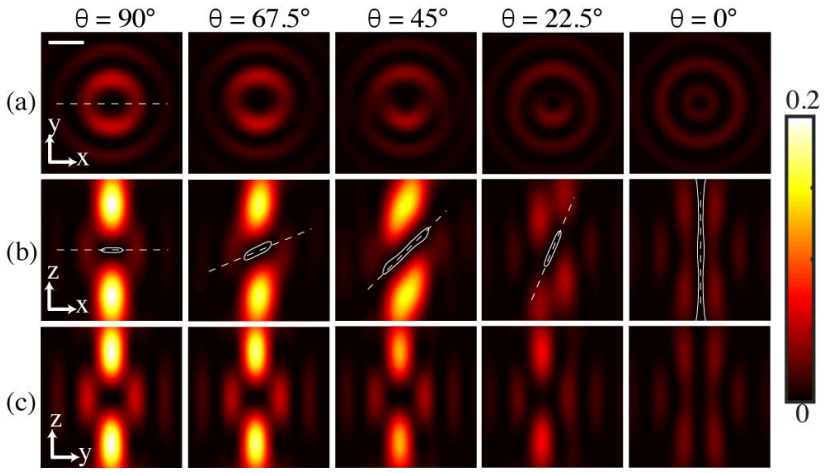

Fig. 5. Simulated ESSat images of a molecule, computed for various orientations of the dipole placed in the (xz) plane and making a polar angle q with the z axis. The images are built in the (xy) plane (a), the (xz) plane (b) and in the (yz) plane (c), for $I_{max} = I_s$, l = 589 nm and NA = 0.95. The scale bar is 500 nm. Iso-intensity contours around the PSF center are plotted in white lines. The dashed lines indicate the dipole orientation. In (b), the dipole orientations coincide with that of the iso-intensity contours.

Figure 6 exemplifies the method to determine the 3D-dipole orientation of a single DBATT molecule. We record two ESSat images at moderate saturations and perform numerical simulations to reproduce them by varying the azimuthal and polar dipole angles j and q. From the transverse image (see Fig. 6a, b), we can extract j . The second image is obtained by scanning the molecule in the longitudinal plane containing the dipole moment and the optical axis. Reproducing the latter image with simulations provides the determination of q, as shown in Fig. 6(c)-(f). For a signal-to-noise ratio of ~30, j and q are determined with an accuracy of $\pm 3°$ and for dipoles nearly parallel to the optical axis z, this accuracy degrades to $\pm 5°$.

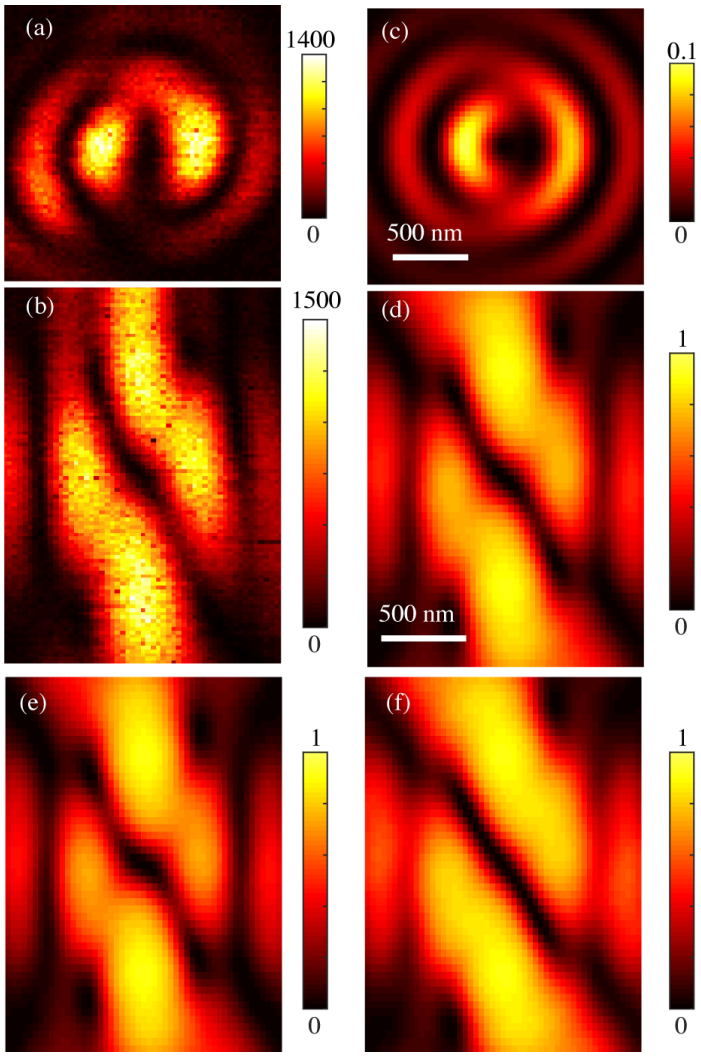

Fig. 6. Determination of the 3D dipole orientation of a single molecule. (a), (c) Experimental ESSat images of a DBATT molecule in octadecane, taken in the (xy) plane (a) and in the (yz) plane (c). From image (a) we deduce $j = 90 \pm 3°$. (b), (d)-(f) Simulated ESSat images, taking $j = 90°$ and $q = 46°$ (d), $q = 49°$ (e), $q = 43°$ (f). From the comparison of simulated to measured image patterns, in particular the regions close to the PSF center, we deduce $q = 46 \pm 3°$. Images are obtained using $I_{max}/I_S = 5$.

With direct ESSat images, the locations of the molecules are given by fluorescence minima. If the emitters are highly concentrated, their fluorescence patterns will overlap, which will degrade the contrast of the images. In order to restore positive contrasts, we overlap on the saturating beam a weak Gaussian beam with a temporally modulated intensity. To avoid optical interferences between these beams, their polarizations are set circular with opposite helicities, and a slight frequency detuning of ~1 MHz (i.e. much smaller than the ZPL linewidth) is applied between them. Then we extract the amplitude of the fluorescence signal modulation, as has been done in 2D-ESSat nanoscopy[23]. Figure 7 displays modulated 3D-ESSat images of a single DBATT molecule in a plane containing the optical axis and in the transverse plane, for increasing excitation intensities of the 0-π beam (see Fig. 7a-c). At strong saturation, 3D super-resolution is achieved with a resolution better than 50 nm (see

Fig. 7d,e,g,h). As in the case of direct 3D-ESSat images, the 3D-orientation of the molecular dipole can be extracted from the analysis of the PSF structure in these planes. For this molecule we find $j = 0°$ and $q = 66°$ and verify a posteriori that the images computed with this dipole orientation (See Fig. 7f,i) are similar to the experimental ones.

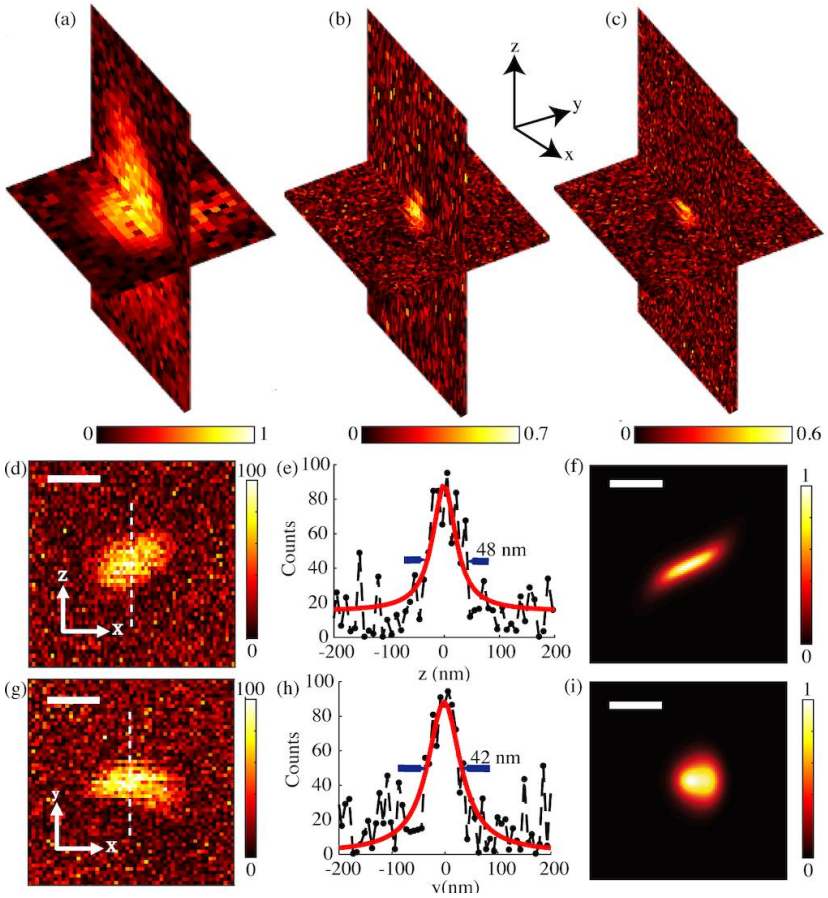

Fig. 7. Modulated 3D-ESSat imaging. Images of a single DBATT molecule embedded in an octadecane matrix, with various intensities of the 0-π beam and a Gaussian beam intensity of 6 W/cm^2 : (a) I_{max} = 16 W/cm^2, (b) I_{max} = 78 W/cm^2, (c) I_{max} = 163 W/cm^2. The colorbar is normalized to the maximal fluorescence count rate in (a). l = 589 nm, pixel dwell time: 5 ms. (d,g) Zooms on the modulated ESSat images displayed in (c). The colobar scale is given in counts per 10 ms. Scale bar: 100 nm. (e,h) Cross sectional profiles of the images in (d,g), respectively, along the two white lines and their associated fits with Lorentzian curves (solid lines). The resolutions (FHWM) are 48 nm along the optical axis and 42 nm in the transverse plane. (f,i) Simulated images performed with the experimental excitation intensities of (d,g) and for a dipole orientation given by $j = 0°$ and $q = 66°$. The modulation signal is derived from the difference between signals calculated with and without the Gaussian beam. The colorbar is given in unit of saturated fluorescence intensity.

6. Achieving sub-30 nm resolutions

Figure 8 provides a comparison between the 3D-reconstructed PSF surfaces of a single DBATT molecule obtained in conventional confocal microscopy (Fig. 8a) and with modulated ESSat imaging (Fig. 8b). The points forming those surfaces are the locations where the fluorescence signal is half of its maximum. In the confocal image recorded with a Gaussian beam, the PSF has a transverse size of 375 nm and a longitudinal size of 900 nm. In the case of modulated 3D-ESSat with the same molecule, the transverse resolution is 55 nm and the longitudinal resolution 29 nm at $I_{max} = 3$ kW/cm^2. This demonstrates a thirty times improvement in the longitudinal resolution. Ultimately, for another molecule, a 3D super-resolved PSF is achieved with transverse and longitudinal resolutions of 28 nm and 22 nm, respectively, at higher saturation with $I_{max} = 10$ kW/cm^2 (see Fig. 8c,d,e).

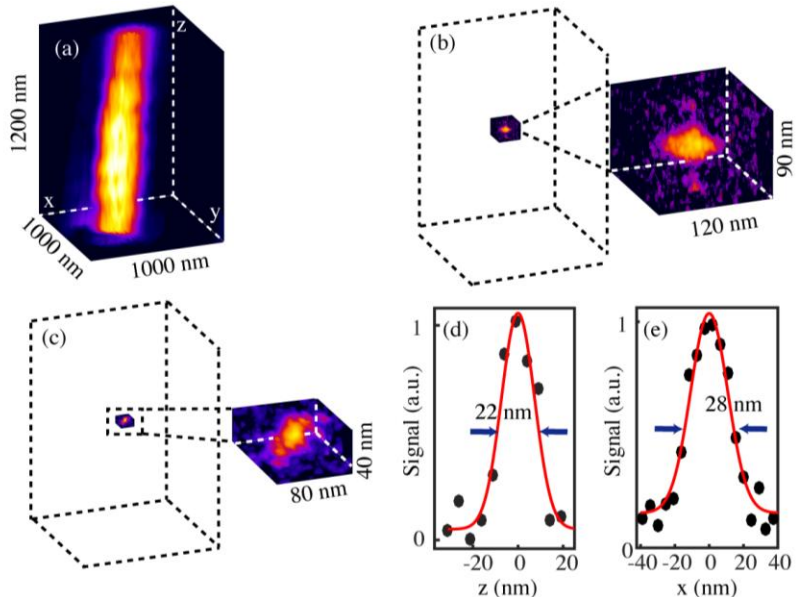

Fig. 8. 3D-reconstruction of the PSF surface, obtained at half of the maximal fluorescence signal of a single DBATT molecule excited at 618 nm. (a) The molecule is imaged in confocal microscopy, with a Gaussian beam with intensity 1.2 W/cm^2. The transverse and longitudinal sizes of the surface are 375 nm and 900 nm, respectively. (b) Modulated-ESSat PSF built for the same molecule, with $I_{max} = 3$ kW/cm^2 and an intensity of the modulated Gaussian beam of 60 W/cm^2. (c) PSF of another molecule, demonstrating transverse and longitudinal resolutions of 28 nm and 22 nm, with $I_{max} = 10$ kW/cm^2 and an intensity of the modulated Gaussian beam of 75 W/cm^2. 3D images plotted with ImageJ (NIH). (d,e) Cross sectional profiles of the 3D-image in (c).

7. Conclusion

In conclusion, we have developed a low temperature optical super-resolution method to image quantum emitters with a sub-30 nm resolution in the three space directions, and with extremely low excitation intensities (of the order of 10 kW/cm^2) compared to room temperature STED nanoscopy methods. Compared to 2D-ESSat nanoscopy, this method provides an enhancement factor of more than 25 in the axial resolution, as well as a determination of the 3D dipole orientation of the emitters with a precision of a few degrees, from a pair of transverse and longitudinal ESSat images. It will enable 3D super-resolution of neighboring emitters with nanometric separations and thus marks an important milestone in the study of the spatial and spectral signatures of their coherent dipole-dipole interaction.

Funding

Idex Bordeaux (LAPHIA Program), Région Nouvelle Aquitaine, Institut universitaire de France.

References:

1. [1] T.E. Northup, R. Blatt, Quantum information transfer using photons, Nature Photonics. 8 (2014) 356–363. doi:10.1038/nphoton.2014.53.
2. [2] W.B. Gao, A. Imamoglu, H. Bernien, R. Hanson, Coherent manipulation, measurement and entanglement of individual solid-state spins using optical fields, Nature Photonics. 9 (2015) 363–373. doi:10.1038/nphoton.2015.58.
3. [3] A. Badolato, K. Hennessy, M. Atatüre, J. Dreiser, E. Hu, P.M. Petroff, et al., Deterministic Coupling of Single Quantum Dots to Single Nanocavity Modes, Science. 308 (2005) 1158–1161. doi:10.1126/science.1109366.
4. [4] M. Arcari, I. Söllner, A. Javadi, S. Lindskov Hansen, S. Mahmoodian, J. Liu, et al., Near-Unity Coupling Efficiency of a Quantum Emitter to a Photonic Crystal Waveguide, Physical Review Letters. 113 (2014) 093603. doi:10.1063/1.3672034.
5. [5] D.E. Chang, A.S. Sørensen, E.A. Demler, M.D. Lukin, A single-photon transistor using nanoscale surface plasmons, Nat Phys. 3 (2007) 807.
6. [6] M.A. Nielsen, I.L. Chuang, Quantum Computation and Quantum Information, Cambridge University Press, 2010.
7. [7] W.E. Moerner, M. Orrit, Illuminating Single Molecules in Condensed Matter, Science. 283 (1999) 1670.
8. [8] J. Berezovsky, M.H. Mikkelsen, N.G. Stoltz, L.A. Coldren, D.D. Awschalom, Picosecond Coherent Optical Manipulation of a Single Electron Spin in a Quantum Dot, Science. 320 (2008) 349.
9. [9] D. Press, T.D. Ladd, B. Zhang, Y. Yamamoto, Complete quantum control of a single quantum dot spin using ultrafast optical pulses, Nature. 456 (2008) 218–221. doi:10.1103/PhysRevB.68.201305.
10. [10] F. Jelezko, J. Wrachtrup, Single defect centres in diamond: A review, Phys. Stat. Sol. (a). 203 (2006) 3207–3225. doi:10.1134/1.1711457.
11. [11] P. Tamarat, A. Maali, B. Lounis, M. Orrit, Ten Years of Single-Molecule Spectroscopy, J. Phys. Chem. A. 104 (2000) 1–16. doi:10.1021/jp992505l.
12. [12] J.-B. Trebbia, P. Tamarat, B. Lounis, Indistinguishable near-infrared single photons from an individual organic molecule, Phys. Rev. A. 82 (2010) 1929. doi:10.1103/PhysRevLett.77.1413.
13. [13] P. Tamarat, B. Lounis, J. Bernard, M. Orrit, S. Kummer, R. Kettner, et al., Pump-Probe Experiments with a Single Molecule: ac-Stark Effect and Nonlinear Optical Response, Physical Review Letters. 75 (1995) 1514–1517. doi:10.1103/PhysRevLett.75.1514.
14. [14] C. Brunel, B. Lounis, P. Tamarat, M. Orrit, Triggered Source of Single Photons based on Controlled Single Molecule Fluorescence, Physical Review Letters. 83 (1999) 2722–2725.
15. [15] P. Tamarat, F. Jelezko, C. Brunel, A. Maali, B. Lounis, M. Orrit, Non-linear optical response of single molecules, Chemical Physics. 245 (1999) 121–132.
16. [16] G. Wrigge, I. Gerhardt, J. Hwang, G. Zumofen, V. Sandoghdar, Efficient coupling of photons to a single molecule and the observation of its resonance fluorescence, Nat Phys. 4 (2008) 60–66.
17. [17] J. Hwang, M. Pototschnig, R. Lettow, G. Zumofen, A. Renn, S. Götzinger, et al., A single-molecule optical transistor, Nature. 460 (2009) 76–80. doi:10.1038/nature08134.
18. [18] C. Hettich, C. Schmid, J. Zitzmann, S. Kühn, I. Gerhardt, V. Sandoghdar, Nanometer Resolution and Coherent Optical Dipole Coupling of Two Individual Molecules, Science. 298 (2002) 385–389.
19. [19] T. Basché, W.E. Moerner, M. Orrit, U.P. Wild, *Single Molecule Optical Detection, Imaging* (VCH, 1996), (n.d.).
20. [20] S.W. Hell, Far-Field Optical Nanoscopy, Science. 316 (2007) 1153–1158. doi:10.1126/science.1137592.
21. [21] B. Huang, M. Bates, X. Zhuang, Super-Resolution Fluorescence Microscopy, Annu. Rev. Biochem. 78 (2009) 993–1016. doi:10.1146/annurev.biochem.77.061906.092014.
22. [22] A.M. van Oijen, J. Köhler, J. Schmidt, M. Müller, G.J. Brackenhoff, 3-Dimensional super-resolution by spectrally selective imaging, Chemical Physics Letters. 292 (1998) 183–187.
23. [23] B. Yang, J.B. Trebbia, R. Baby, P. Tamarat, B. Lounis, Optical nanoscopy with excited state saturation at liquid helium temperatures, Nature Photonics. 9 (2015) 658–662. doi:10.1038/nphoton.2015.152.
24. [24] S. Li, C. Kuang, X. Hao, Z. Gu, X. Liu, Generation of a 3D isotropic hollow focal spot for single-objective stimulated emission depletion microscopy, J. Opt. 14 (2012) 085704. doi:10.1088/2040-8978/14/8/085704.
25. [25] B. Richards, E. Wolf, Electromagnetic diffraction in optical systems II. Structure of the image field in an aplanatic system, Proceedings of the Royal Society of London. Series a. Mathematical and Physical Sciences. 253 (1959) 358–379.
26. [26] A.S. Marathay, J.F. McCalmont, Vector diffraction theory for electromagnetic waves, J Opt Soc Am A. 18 (2001) 2585–2593.
27. [27] T.J. Gould, D. Burke, J. Bewersdorf, M.J. Booth, Adaptive optics enables 3D STED microscopy in aberrating specimens, Optics Express. 20 (2012) 20998–21009. doi:10.1364/OE.20.020998.

28. [28] M.P. Backlund, M.D. Lew, A.S. Backer, S.J. Sahl, W.E. Moerner, The Role of Molecular Dipole Orientation in Single-Molecule Fluorescence Microscopy and Implications for Super-Resolution Imaging, ChemPhysChem. 15 (2013) 587–599. doi:10.1016/j.bpj.2011.07.008.
29. [29] T. Ha, T.A. Laurence, D.S. Chemla, S. Weiss, Polarization Spectroscopy of Single Fluorescent Molecules, J. Phys. Chem. B. 103 (1999) 6839–6850. doi:10.1021/jp990948j.
30. [30] J.N. Forkey, M.E. Quinlan, Y.E. Goldman, Measurement of Single Macromolecule Orientation by Total Internal Reflection Fluorescence Polarization Microscopy, Biophysical Journal. 89 (2005) 1261–1271. doi:10.1529/biophysj.104.053470.
31. [31] R.M. Dickson, D.J. Norris, W.E. Moerner, Simultaneous Imaging of Individual Molecules Aligned Both Parallel and Perpendicular to the Optic Axis, Physical Review Letters. 81 (1998) 5322–5325.
32. [32] B. Sick, B. Hecht, U.P. Wild, L. Novotny, Probing confined fields with single molecules and vice versa, J Microsc. 202 (2001) 365–373.